ELSEVIER

Comput. Methods Appl. Mech. Engrg. 191 (2002) 1173–1187

Computer methods in applied mechanics and engineering

www.elsevier.com/locate/cma

Simple and effective elements based upon Timoshenko–Mindlin shell theory

G.M. Kulikov *, S.V. Plotnikova

Department of Applied Mathematics and Mechanics, Tambov State Technical University, Sovetskaya Street 106, Tambov 392000, Russia

Received 12 May 2000; received in revised form 29 June 2001

Abstract

The simple and effective mixed models are developed for the analysis of multilayered anisotropic Timoshenko–Mindlin-type shells. The effects of the transverse shear and transverse normal strains, and laminated anisotropic material response are included. The precise representation of rigid body motions in the displacement patterns of curved shell elements is considered. This consideration requires the development of the strain–displacement equations of the Timoshenko–Mindlin-type theory with regard to their consistency with the rigid body motions. The fundamental unknowns consist of six displacements and eleven strains of the face surfaces of the shell, and 11 stress resultants. The element characteristic arrays are obtained by using the Hu–Washizu mixed variational principle. Numerical results are presented to demonstrate the high accuracy and effectiveness of the developed mixed models and to compare their performance with other finite-element models reported in the literature. © 2002 Elsevier Science B.V. All rights reserved.

Keywords: Elasticity; Mixed models; Rigid body motions; Composite shell

1. Introduction

One of the main requirements of a finite element that is intended for general application is that it must lead to strain-free modes for rigid body motions. The adequate representation of rigid body motions is a necessary condition if an element is to have good accuracy and convergence properties. Therefore, when an inconsistent theory is used to construct any finite element, erroneous straining modes under rigid body motions may appear. This problem has been studied for the Kirchhoff–Love shell theory by Cantin [8] and Dawe [10].

Herein, the more general study on the basis of the refined Timoshenko–Mindlin-type (TMT) shell theory taking into account the transverse normal deformation response is considered [20,22]. The direct use of the traditional TMT shell theory [12,23,25,27,29] for solving a series of important shell problems such as the contact problems is not always convenient. In these problems it is more convenient to select as unknown functions the displacements of the face surfaces of the shell [20,22], since with the help of these displacements the kinematic requirement of no penetration of the contact bodies can be fulfilled. Furthermore, the proposed TMT shell theory can also simplify a formulation of new finite-element models.

Using the traditional TMT shell theory in a finite-element formulation for plates and shells is well established and has been shown to give acceptable results [1–7,13–16,24,31,32]. This theory has the advantage

* Corresponding author. Fax: +7-075-271-0216.
E-mail address: kulikov@apmath.tstu.ru (G.M. Kulikov).

0045-7825/02/$ - see front matter
PII: S0045-7825(01)00320-6

that independent displacement and rotation trial functions may be used and these functions need only to be C^0 continuous. The developed refined TMT shell theory has the essential advantage, since only independent displacement trial functions may be used.

Our finite-element formulation is based on a simple and efficient approximation of shells via quadrilateral finite elements developed by Hughes and Tezduyar [16], and by Wempner et al. [31]. The fundamental unknowns consist of six displacements and 11 strains of the face surfaces of a shell, and 11 stress resultants. The simplest admissible approximations of the two-dimensional fields are used: bilinear approximations of the displacements and piecewise constant approximations of the strains and stress resultants. In this connection the elemental arrays are obtained by applying the Hu–Washizu mixed variational principle. It is worth noting that the resulting stiffness matrix has six, and only six, zero eigenvalues as required for satisfaction of the general rigid body motion requirements, and the element does not contain any spurious zero energy modes.

Numerical results are presented to demonstrate the high accuracy and effectiveness of the finite-element models developed and to compare their performance with other finite-element models. For this purpose four tests are employed. They are thin square and rectangular plates, a pinched cylinder, an open cylindrical shell segment roof, and an open cylindrical composite shell.

2. Strain–displacement equations

Let us consider the shell of the uniform thickness h. The shell may be defined as a three-dimensional body of volume V bounded by two bounding surfaces S^- and S^+, located at the distances δ^- and δ^+ measured with respect to the reference surface S, and the edge boundary surface Ω that is perpendicular to the reference surface (see Fig. 1). Let the reference surface S be referred to an orthogonal curvilinear coordinate system α_1 and α_2 which coincides with the lines of principal curvatures of its surface. The α_3 axis is oriented along the outward unit vector $\mathbf{e}_3$ normal to the reference surface.

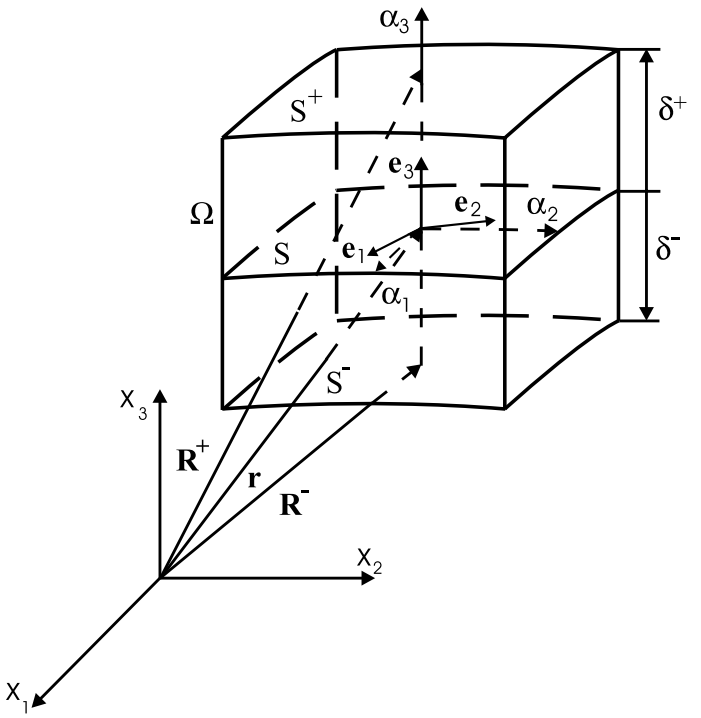

Fig. 1. Shell element.

The three-dimensional strain–displacement relationships for the *thick* shell in a vector form can be written as

$$\varepsilon_{ii} = \frac{1}{H_i}\frac{\partial \mathbf{u}}{\partial \alpha_i}\mathbf{e}_i, \quad \varepsilon_{ij} = \frac{1}{H_i}\frac{\partial \mathbf{u}}{\partial \alpha_i}\mathbf{e}_j + \frac{1}{H_j}\frac{\partial \mathbf{u}}{\partial \alpha_j}\mathbf{e}_i \quad (i \neq j), \quad H_\alpha = A_\alpha(1 + k_\alpha \alpha_3), \quad H_3 = 1, \tag{1}$$

where $\mathbf{u} = \sum_i u_i \mathbf{e}_i$ is the displacement vector; $u_i(\alpha_1, \alpha_2, \alpha_3)$ are the components of this vector, $\mathbf{e}_\alpha$ and $\mathbf{e}_3$ are the tangent and normal unit vectors of the reference surface, A_α and k_α are the Lamé coefficients and principal curvatures of the reference surface. Both here and in the following developments, unless otherwise specified, Greek indices may take the values 1, 2 while Latin indices take the values 1, 2, 3.

The refined TMT shell theory is based on the linear approximation of the displacement vector in the thickness direction [20,22]

$$\mathbf{u} = N^-(\alpha_3)\mathbf{v}^- + N^+(\alpha_3)\mathbf{v}^+, \quad N^-(\alpha_3) = \left(\delta^+ - \alpha_3\right)/h, \quad N^+(\alpha_3) = (\alpha_3 - \delta^-)/h, \tag{2}$$

where $\mathbf{v}^\pm = \sum_i v_i^\pm \mathbf{e}_i$ are the displacement vectors of the face surfaces $S^\pm$, $v_i^\pm(\alpha_1, \alpha_2)$ are the displacements of the face surfaces; $N^-(\alpha_3)$ and $N^+(\alpha_3)$ are the linear shape functions. The linear approximation (2) may be considered as a refined Timoshenko kinematic hypothesis (see, for example, monograph [12], where as unknown functions the displacements and rotation components of the reference surface are selected). The advantage of the proposed approach is obvious, since with the help of the displacements $v_i^\pm$ the kinematic boundary conditions on the face surfaces of the shell, and in particular, the conditions of no penetration of the contact bodies can be formulated. Moreover, this simplifies a formulation of new finite-element models and provides a convenient way to express the non-linear strain–displacement relationships in terms of face surface strains [19,22].

Substituting the displacements (2) into the strain–displacement relationships (1) and replacing the Lamé coefficients H_α by their values on the top and bottom surfaces $H_\alpha^\pm = A_\alpha\left(1 + k_\alpha \delta^\pm\right)$ in expressions for the tangential strains and by their values on the middle surface $\bar{H}_\alpha = A_\alpha\left(1 + k_\alpha \bar{\delta}\right)$ in expressions for the transverse shear strains, the following equations of the refined TMT theory of the *moderately thick* shells are obtained:

$$\begin{aligned}
\hat{\varepsilon}_{\gamma\gamma} &= \left(N^-(\alpha_3)\frac{1}{H_\gamma^-}\frac{\partial \mathbf{v}^-}{\partial \alpha_\gamma} + N^+(\alpha_3)\frac{1}{H_\gamma^+}\frac{\partial \mathbf{v}^+}{\partial \alpha_\gamma}\right)\mathbf{e}_\gamma, \quad \hat{\varepsilon}_{33} = \boldsymbol{\beta}\mathbf{e}_3, \\
\hat{\varepsilon}_{12} &= \left(N^-(\alpha_3)\frac{1}{H_1^-}\frac{\partial \mathbf{v}^-}{\partial \alpha_1} + N^+(\alpha_3)\frac{1}{H_1^+}\frac{\partial \mathbf{v}^+}{\partial \alpha_1}\right)\mathbf{e}_2 + \left(N^-(\alpha_3)\frac{1}{H_2^-}\frac{\partial \mathbf{v}^-}{\partial \alpha_2} + N^+(\alpha_3)\frac{1}{H_2^+}\frac{\partial \mathbf{v}^+}{\partial \alpha_2}\right)\mathbf{e}_1, \\
\hat{\varepsilon}_{\gamma 3} &= \boldsymbol{\beta}\mathbf{e}_\gamma + \frac{1}{\bar{H}_\gamma}\frac{\partial \mathbf{v}}{\partial \alpha_\gamma}\mathbf{e}_3 + (\alpha_3 - \bar{\delta})\frac{1}{\bar{H}_\gamma}\frac{\partial \hat{\varepsilon}_{33}}{\partial \alpha_\gamma}, \quad \boldsymbol{\beta} = \frac{1}{h}(\mathbf{v}^+ - \mathbf{v}^-), \quad \mathbf{v} = \frac{1}{2}(\mathbf{v}^- + \mathbf{v}^+),
\end{aligned} \tag{3}$$

where $\bar{\delta} = (\delta^- + \delta^+)/2$ is the distance from the reference surface to the middle surface of the shell.

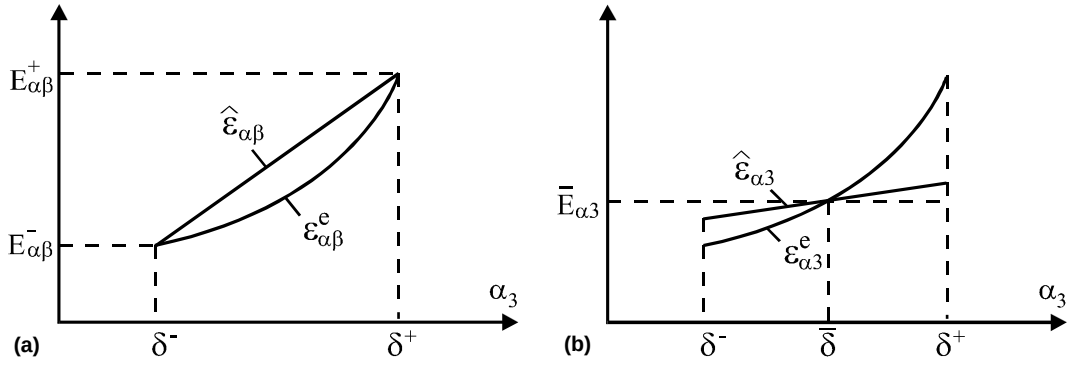

Fig. 2. Distribution of: (a) tangential strains and (b) transverse shear strains over shell thickness.

Note that the tangential strains $\hat{\varepsilon}_{\alpha\beta}$ are distributed over the shell thickness according to the linear law. As can be seen in Fig. 2(a), it is an acceptable assumption for the *moderately thick* shells. Really, better ('exact') expressions for the tangential strains $\varepsilon^{e}_{\alpha\beta}$ can be written by using more general non-linear approximations, since the Lamé coefficients H_α depend on the normal coordinate α_3. But, taking into account that the coupling conditions $\varepsilon^{e}_{\alpha\beta}(\delta^{\pm}) = \hat{\varepsilon}_{\alpha\beta}(\delta^{\pm}) = E^{\pm}_{\alpha\beta}$ are satisfied, this complication of the TMT shell theory would be unreasonable. The transverse shear strains are also distributed over the shell thickness according to the linear law. However, in this case the coupling conditions have the traditional form $\varepsilon^{e}_{\alpha 3}(\bar{\delta}) = \hat{\varepsilon}_{\alpha 3}(\bar{\delta}) = \bar{E}_{\alpha 3}$, where $\varepsilon^{e}_{\alpha 3}$ are the exact expressions for the transverse shear strains (see Fig. 2(b)).

More simple strain–displacement equations can be obtained for the thin shells by substituting the displacements (2) into the strain–displacement relationships (1) and replacing the Lamé coefficients of the shell H_α by the Lamé coefficients of the reference surface A_α. As a result we have

$$\begin{aligned}
&\tilde{\varepsilon}_{\gamma\gamma} = \left(N^{-}(\alpha_3)\frac{1}{A_\gamma}\frac{\partial \mathbf{v}^{-}}{\partial \alpha_\gamma} + N^{+}(\alpha_3)\frac{1}{A_\gamma}\frac{\partial \mathbf{v}^{+}}{\partial \alpha_\gamma}\right)\mathbf{e}_\gamma, \quad \tilde{\varepsilon}_{33} = \boldsymbol{\beta}\mathbf{e}_3,\\
&\tilde{\varepsilon}_{12} = \left(N^{-}(\alpha_3)\frac{1}{A_1}\frac{\partial \mathbf{v}^{-}}{\partial \alpha_1} + N^{+}(\alpha_3)\frac{1}{A_1}\frac{\partial \mathbf{v}^{+}}{\partial \alpha_1}\right)\mathbf{e}_2 + \left(N^{-}(\alpha_3)\frac{1}{A_2}\frac{\partial \mathbf{v}^{-}}{\partial \alpha_2} + N^{+}(\alpha_3)\frac{1}{A_2}\frac{\partial \mathbf{v}^{+}}{\partial \alpha_2}\right)\mathbf{e}_1,\\
&\tilde{\varepsilon}_{\gamma 3} = \boldsymbol{\beta}\mathbf{e}_\gamma + \frac{1}{A_\gamma}\frac{\partial \mathbf{v}}{\partial \alpha_\gamma}\mathbf{e}_3 + (\alpha_3 - \bar{\delta})\frac{1}{A_\gamma}\frac{\partial \tilde{\varepsilon}_{33}}{\partial \alpha_\gamma}, \quad \boldsymbol{\beta} = \frac{1}{h}(\mathbf{v}^{+} - \mathbf{v}^{-}), \quad \mathbf{v} = \frac{1}{2}(\mathbf{v}^{-} + \mathbf{v}^{+}).
\end{aligned} \tag{4}$$

Consider a limit case. If the transverse displacement u_3 is independent on the normal coordinate α_3, i.e., $v_3^{-} = v_3^{+} = v_3$ then transverse shear strains $\hat{\varepsilon}_{\alpha 3}$ and $\tilde{\varepsilon}_{\alpha 3}$ are also independent on the normal coordinate. This statement is true for the classical TMT shell theory.

3. Rigid body motions

A small rigid body motion is defined as [11]

$$\mathbf{u}_r = \boldsymbol{\Delta} + \boldsymbol{\Phi} \times \mathbf{R}, \tag{5}$$

where $\boldsymbol{\Delta} = \sum_i \Delta_i \mathbf{e}_i$ is the constant displacement (translation) vector, $\boldsymbol{\Phi} = \sum_i \Phi_i \mathbf{e}_i$ is the constant rotation vector, $\mathbf{R} = \mathbf{r} + \alpha_3 \mathbf{e}_3$ is the position vector of any point of the shell, $\mathbf{r}$ is the position vector of any point of the reference surface (see Fig. 1). In particular, rigid body motions of the face surfaces are

$$\mathbf{v}_r^{\pm} = \boldsymbol{\Delta} + \boldsymbol{\Phi} \times \mathbf{R}^{\pm}, \tag{6}$$

where $\mathbf{R}^{\pm} = \mathbf{r} + \delta^{\pm}\mathbf{e}_3$ are the position vectors of points of the top and bottom surfaces.

The derivatives of the translation and rotation vectors with respect to the reference surface coordinates are zero, i.e.,

$$\frac{\partial \boldsymbol{\Delta}}{\partial \alpha_\gamma} = \mathbf{0}, \quad \frac{\partial \boldsymbol{\Phi}}{\partial \alpha_\gamma} = \mathbf{0}. \tag{7}$$

Taking into account the formulas for the derivatives of the unit vectors $\mathbf{e}_i$ along the coordinate lines [11] and using the Eqs. (6) and (7), one can obtain the following expressions for the derivatives:

$$\frac{\partial \mathbf{v}_r^{\pm}}{\partial \alpha_\gamma} = H_\gamma^{\pm} \boldsymbol{\Phi} \times \mathbf{e}_\gamma. \tag{8}$$

It can be verified by using Eqs. (6) and (8) that the strains given by Eq. (3) are all zero in a general rigid body motion, i.e.,

$$\tilde{\varepsilon}^r_{ii} = (\mathbf{\Phi} \times \mathbf{e}_i)\mathbf{e}_i = 0, \quad \tilde{\varepsilon}^r_{ij} = 0 \quad (i \neq j).$$

So, the TMT theory of *moderately thick* shells is completely strain-free for all rigid body motions.

Using again Eqs. (6) and (8) into the strain–displacement relationships (4), one can get the following results:

$$\tilde{\varepsilon}^r_{\alpha\alpha} = (1 + k_\alpha \alpha_3)(\mathbf{\Phi} \times \mathbf{e}_\alpha)\mathbf{e}_\alpha = 0, \quad \tilde{\varepsilon}^r_{33} = (\mathbf{\Phi} \times \mathbf{e}_3)\mathbf{e}_3 = 0,$$
$$\tilde{\varepsilon}^r_{12} = (k_1 - k_2)\alpha_3(\mathbf{\Phi} \times \mathbf{e}_1)\mathbf{e}_2, \qquad \tilde{\varepsilon}^r_{\alpha 3} = k_\alpha \bar{\delta}(\Phi \times \mathbf{e}_\alpha)\mathbf{e}_3$$

showing that rigid body motions can never be completely strain-free for the TMT theory of *thin* shells. However, the transverse shear strains $\tilde{\varepsilon}^r_{\alpha 3} = 0$ when a reference surface is selected to be the middle surface, since in this case $\bar{\delta} = 0$. The tangential shear strain $\tilde{\varepsilon}^r_{12} = 0$ in the case of a spherical shell or a symmetrically loaded and supported isotropic or orthotropic shell of revolution, and at the reference surface points of anisotropic shells of arbitrary geometry.

4. Hu–Washizu functional

Let us consider the shell built up in the general case by the arbitrary superposition across the wall thickness of N thin layers of uniform thickness h_k. The kth layer may be defined as a three-dimensional body of volume V_k bounded by two surfaces S_{k-1} and S_k, located at the distances δ_{k-1} and δ_k measured with respect to the reference surface S, and the edge boundary surface Ω_k that is perpendicular to the reference

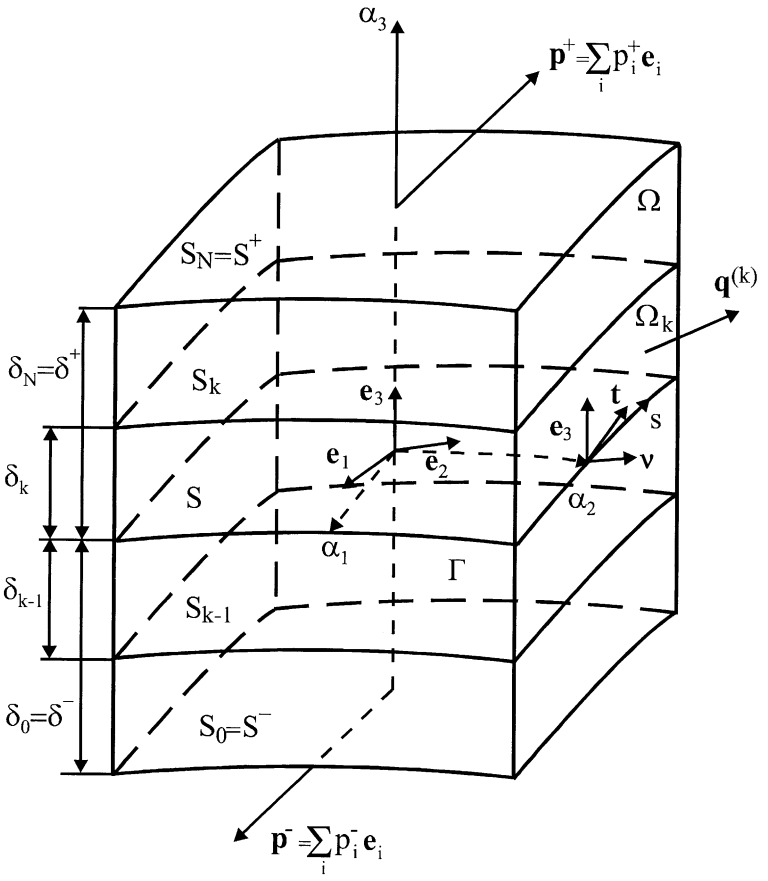

Fig. 3. Multilayered shell element.

surface (see Fig. 3). Here and in the following developments the index k identifies the belonging of any quantity to the kth layer. The full edge boundary surface $\Omega = \Omega_1 + \Omega_2 + \cdots + \Omega_N$ is generated by the normals to the reference surface along the bounding curve Γ (with the arc length s) of this surface. It is also assumed that the bounding surfaces S_{k-1} and S_k are continuous, sufficiently smooth and without any singularities. Let the reference surface be referred to an orthogonal curvilinear coordinate system α_1 and α_2 that coincides with the lines of principal curvatures of its surface. The α_3 axis is oriented along the outward unit vector $\mathbf{e}_3$ normal to the reference surface.

The constituent layers of the shell are supposed to be rigidly joined, so that no slip on contact surfaces and no separation of layers can occur. The material of each constituent layer is assumed to be linearly elastic, anisotropic and homogeneous or fiber reinforced, such that in each point there is a single surface of elastic symmetry parallel to the reference surface. Let p_i^- and p_i^+ be the intensities of the external loading acting on the bottom surface $S^- = S_0$ and top surface $S^+ = S_N$ in the α_i coordinate directions, respectively; $\mathbf{q}^{(k)} = \mathrm{q}_v^{(k)}\boldsymbol{\nu} + q_t^{(k)}\mathbf{t} + q_3^{(k)}\mathbf{e}_3$ is the external loading vector acting on the edge boundary surface Ω_k; $q_v^{(k)}$, $q_t^{(k)}$ and $q_3^{(k)}$ are the components of its vector acting in the ν, t and z directions; $\boldsymbol{\nu}$ and $\mathbf{t}$ are the normal and tangential unit vectors to the bounding curve Γ.

The refined TMT theory of multilayered shells is also based on the linear approximation of the displacement vector in the thickness direction (2), where we should set $\delta^- = \delta_0$ and $\delta^+ = \delta_N$. Substituting the displacements (2) and strains rewritten in the more convenient form

$$\hat{\varepsilon}_{\alpha\beta} = N^-(\alpha_3)E^-_{\alpha\beta} + N^+(\alpha_3)E^+_{\alpha\beta}, \quad \hat{\varepsilon}_{\alpha 3} = N^-(\alpha_3)E^-_{\alpha 3} + N^+(\alpha_3)E^+_{\alpha 3}, \quad \hat{\varepsilon}_{33} = E_{33} \tag{9}$$

into the Hu–Washizu functional [18,21] and accounting for the strain–displacement relationships (3), one can obtain

$$\begin{aligned} J = \int\int_S \Bigg\{ \Pi - \sum_{\alpha\leqslant\beta}\Big[H^-_{\alpha\beta}\Big(E^-_{\alpha\beta} - e^-_{\alpha\beta}\Big) + H^+_{\alpha\beta}\Big(E^+_{\alpha\beta} - e^+_{\alpha\beta}\Big)\Big] \\ - \sum_{\alpha}\big[H^-_{\alpha 3}\big(E^-_{\alpha 3} - e^-_{\alpha 3}\big) + H^+_{\alpha 3}\big(E^+_{\alpha 3} - e^+_{\alpha 3}\big)\big] - H_{33}(E_{33} - e_{33}) - \sum_i\big[\big(Q_i^- - p_i^-\big)v_i^- + \big(Q_i^+ + p_i^+\big)v_i^+\big] \Bigg\}\mathrm{d}S \\ - \oint_\Gamma \Big(\hat{H}^-_{vv}v_v^- + \hat{H}^+_{vv}v_v^+ + \hat{H}^-_{vt}v_t^- + \hat{H}^+_{vt}v_t^+ + \hat{H}^-_{v3}v_3^- + \hat{H}^+_{v3}v_3^+\Big)\mathrm{d}s, \end{aligned} \tag{10}$$

$$e^\pm_{\gamma\gamma} = \frac{1}{\varsigma^\pm_\gamma}\left(\frac{1}{A_\gamma}\frac{\partial v^\pm_\gamma}{\partial\alpha_\gamma} + B_\delta v^\pm_\delta + k_\gamma v^\pm_3\right), \quad e^\pm_{12} = \frac{1}{\varsigma^\pm_1}\left(\frac{1}{A_1}\frac{\partial v^\pm_2}{\partial\alpha_1} - B_2 v^\pm_1\right) + \frac{1}{\varsigma^\pm_2}\left(\frac{1}{A_2}\frac{\partial v^\pm_1}{\partial\alpha_2} - B_1 v^\pm_2\right),$$

$$e^\pm_{\gamma 3} = \left(1 \pm \frac{k_\gamma h}{2\bar{\varsigma}_\gamma}\right)\beta_\gamma - \frac{1}{\bar{\varsigma}_\gamma}\theta^\pm_\gamma, \quad e_{33} = \beta_3, \quad \theta^\pm_\gamma = k_\gamma v^\pm_\gamma - \frac{1}{A_\gamma}\frac{\partial v^\pm_3}{\partial\alpha_\gamma}, \quad \beta_i = \frac{1}{h}\big(v_i^+ - v_i^-\big),$$

$$\varsigma^\pm_\gamma = 1 + k_\gamma\delta^\pm, \quad \bar{\varsigma}_\gamma = 1 + k_\gamma\bar{\delta}, \quad B_\gamma = \frac{1}{A_1A_2}\frac{\partial A_\delta}{\partial\alpha_\gamma} \quad (\gamma \neq \delta),$$

where Π is the strain energy density; $v^\pm_\nu$,$v^\pm_t$ and $v^\pm_3$ are the components of the displacement vectors of the face surfaces in the coordinate system ν, t and α_3 (see Fig. 3), $E^\pm_{\alpha\beta}$ and $E^\pm_{\alpha 3}$ are the tangential strains and transverse shear strains of the face surfaces; E_{33} is the transverse normal strain of the reference surface; $H^\pm_{\alpha\beta}$ and $H^\pm_{\alpha 3}$ are the generalized stress resultants; H_{33} is the classical stress resultant, $Q^\pm_i$ are the generalized body force resultants; $H^\pm_{\nu\nu}$, $H^\pm_{\nu t}$ and $H^\pm_{\nu 3}$ are the generalized external load resultants, which are defined as

$$\Pi = \frac{1}{2}\sum_{i\leqslant j,\ell\leqslant m}\Big[A^{00}_{ij\ell m}E^-_{ij}E^-_{\ell m} + A^{01}_{ij\ell m}\Big(E^-_{ij}E^+_{\ell m} + E^+_{ij}E^-_{\ell m}\Big) + A^{11}_{ij\ell m}E^+_{ij}E^+_{\ell m}\Big], \tag{11}$$

$$A^{pq}_{ij\ell m} = \sum_{k=1}^{N}\int_{\delta_{k-1}}^{\delta_k} C^{(k)}_{ij\ell m}(N^-(\alpha_3))^{2-p-q}(N^+(\alpha_3))^{p+q}\mathrm{d}\alpha_3 \quad (p,q = 0,1), \tag{12}$$

$$
\begin{aligned}
&H_{\alpha i}^{\pm}=\sum_{k=1}^{N}\int_{\delta_{k-1}}^{\delta_k}\sigma_{\alpha i}^{(k)}N^{\pm}(\alpha_3)\mathrm{d}\alpha_3, \qquad H_{33}=\sum_{k=1}^{N}\int_{\delta_{k-1}}^{\delta_k}\sigma_{33}^{(k)}\mathrm{d}\alpha_3,\\
&Q_i^{\pm}=\sum_{k=1}^{N}\int_{\delta_{k-1}}^{\delta_k}f_i^{(k)}N^{\pm}(\alpha_3)\mathrm{d}\alpha_3, \quad \hat{H}_{vs}^{\pm}=\sum_{k=1}^{N}\int_{\delta_{k-1}}^{\delta_k}q_s^{(k)}N^{\pm}(\alpha_3)\mathrm{d}\alpha_3 \quad (s=v,t,3),
\end{aligned}
\tag{13}
$$

where $C_{ij\ell m}^{(k)}$ are the stiffness coefficients of the kth layer; $f_i^{(k)}$ are the externally applied body forces of the kth layer. Besides, we should set into relationships (11) and (12) $E_{33}^{-}=E_{33}^{+}=E_{33}$ and $C_{\alpha\beta\gamma 3}^{(k)}=C_{\alpha 333}^{(k)}=0$.

5. Finite-element formulation

It is well known that the Hu–Washizu variational principle provides the basis for the derivation of various variational principles, and many different mixed and hybrid finite elements can be designed [26]. Herein, the Hu–Washizu functional (10)–(13) for the element e can be written in the following form:

$$
\begin{aligned}
&J^{\mathrm{e}}=\int_{-1}^{1}\int_{-1}^{1}\left[\tfrac{1}{2}\mathbf{E}^{\mathrm{T}}\mathbf{A}\mathbf{E}-\left(\mathbf{E}^{\mathrm{T}}-\mathbf{v}^{\mathrm{T}}\mathbf{B}^{\mathrm{T}}\right)\mathbf{H}-\mathbf{v}^{\mathrm{T}}(\mathbf{P}+\mathbf{Q})\right]\Lambda\mathrm{d}\xi_1\mathrm{d}\xi_2-\oint_{\Gamma^{\mathrm{e}}}\mathbf{v}_{\Gamma}^{\mathrm{T}}\hat{\mathbf{H}}_{\Gamma}\mathrm{d}s,\\
&\mathbf{H}=[H_{11}^{-}\ H_{11}^{+}\ H_{12}^{-}\ H_{12}^{+}\ H_{22}^{-}\ H_{22}^{+}\ H_{13}^{-}\ H_{13}^{+}\ H_{23}^{-}\ H_{23}^{+}\ H_{33}]^{\mathrm{T}},\\
&\mathbf{E}=[E_{11}^{-}\ E_{11}^{+}\ E_{12}^{-}\ E_{12}^{+}\ E_{22}^{-}\ E_{22}^{+}\ E_{13}^{-}\ E_{13}^{+}\ E_{23}^{-}\ E_{23}^{+}\ E_{33}]^{\mathrm{T}},
\end{aligned}
\tag{14}
$$

where ξ_1 and ξ_2 are the local coordinates of the element that vary from -1 to $+1$, $\Lambda(\xi_1,\xi_2)$ is the function characterizing the metric of the element, $\mathbf{v}=[v_1^{-}\ v_1^{+}\ v_2^{-}\ v_2^{+}\ v_3^{-}\ v_3^{+}]^{\mathrm{T}}$ is the displacement vector, $\mathbf{v}_{\Gamma}=[v_{\nu}^{-}\ v_{\nu}^{+}\ v_{t}^{-}\ v_{t}^{+}\ v_{3}^{-}\ v_{3}^{+}]^{\mathrm{T}}$ is the displacement vector of the element edge Γ^{e}, $\mathbf{E}$ is the strain vector, $\mathbf{H}$ is the stress resultant vector, $\hat{\mathbf{H}}_{\Gamma}=[\hat{H}_{\nu\nu}^{-}\ \hat{H}_{\nu\nu}^{+}\ \hat{H}_{\nu t}^{-}\ \hat{H}_{\nu t}^{+}\ \hat{H}_{\nu 3}^{-}\ \hat{H}_{\nu 3}^{+}]^{\mathrm{T}}$ is the stress resultant vector acting on the element edge Γ^{e}, $\mathbf{Q}=[Q_1^{-}\ Q_1^{+}\ Q_2^{-}\ Q_2^{+}\ Q_3^{-}\ Q_3^{+}]^{\mathrm{T}}$ is the body force resultant vector, $\mathbf{P}=[-p_1^{-}\ p_1^{+}-p_2^{-}\ p_2^{+}-p_3^{-}\ p_3^{+}]^{\mathrm{T}}$ is the surface traction vector acting on the element surface S^{e}, $\mathbf{A}$ is the generalized stiffness matrix, $\mathbf{B}$ is the strain–displacement matrix.

For the quadrilateral 4-node shell element the displacement field is approximated according to the standard C^0 interpolation

$$
\mathbf{v}=\sum_{r=1}^{4}N_r\mathbf{v}_r,
\tag{15}
$$

where $N_r(\xi_1,\xi_2)$ are the shape functions of the element e; $\mathbf{v}_r=[v_{1,r}^{-}\ v_{1,r}^{+}\ v_{2,r}^{-}\ v_{2,r}^{+}\ v_{3,r}^{-}\ v_{3,r}^{+}]^{\mathrm{T}}$ are the displacement vectors of the element nodes.

In accordance with Hughes and Tezduyar [16], Wempner et al. [31], and Betsch and Stein [6] the following strain interpolations are adopted:

$$
\begin{aligned}
&\mathbf{E}=\sum_{r_1,r_2=0}^{1}\mathbf{E}^{r_1r_2}\xi_1^{r_1}\xi_2^{r_2},\\
&\mathbf{E}^{00}=[E_{11}^{-00}\ E_{11}^{+00}\ E_{12}^{-00}\ E_{12}^{+00}\ E_{22}^{-00}\ E_{22}^{+00}\ E_{13}^{-00}\ E_{13}^{+00}\ E_{23}^{-00}\ E_{23}^{+00}\ E_{33}^{00}]^{\mathrm{T}},\\
&\mathbf{E}^{10}=[0\ 0\ 0\ 0\ E_{22}^{-10}\ E_{22}^{+10}\ 0\ 0\ E_{23}^{-10}\ E_{23}^{+10}\ E_{33}^{10}]^{\mathrm{T}},\\
&\mathbf{E}^{01}=[E_{11}^{-01}\ E_{11}^{+01}\ 0\ 0\ 0\ 0\ E_{13}^{-01}\ E_{13}^{+01}\ 0\ 0\ E_{33}^{01}]^{\mathrm{T}},\\
&\mathbf{E}^{11}=[0\ 0\ 0\ 0\ 0\ 0\ 0\ 0\ 0\ 0\ E_{33}^{11}]^{\mathrm{T}},
\end{aligned}
\tag{16}
$$

where $\mathbf{E}^{00}$ is the vector of homogeneous states of strains; $\mathbf{E}^{10},\mathbf{E}^{01}$ and $\mathbf{E}^{11}$ are the vectors of the higher approximation modes of strains. The interpolations of the stress resultants follow the forms of the corresponding strains

$$\mathbf{H} = \sum_{r_1,r_2=0}^{1} \mathbf{H}^{r_1 r_2} \xi_1^{r_1} \xi_2^{r_2}, \tag{17}$$

where the vectors $\mathbf{H}^{r_1 r_2}$ are defined by replacing a letter E by a letter H.

Note that the 24 modes of our element are the six rigid body motions, the eleven homogeneous states of strains $E_{\alpha\beta}^{\pm 00}, E_{\alpha 3}^{\pm 00}, E_{33}^{00}$ and the seven additional modes representing higher approximations of strains $E_{11}^{\pm 01}, E_{22}^{\pm 10}, E_{13}^{\pm 01}, E_{23}^{-10}$. Indeed, from the relationships (10), (15), (16) the four coupling equations are derived:

$$\begin{aligned} &A_1\bar{\varsigma}_1\left(E_{13}^{+01} - E_{13}^{-01}\right) = A_2\bar{\varsigma}_2\left(E_{23}^{+10} - E_{23}^{-10}\right), \quad hE_{33}^{11} = A_1\bar{\varsigma}_1\left(E_{13}^{+01} - E_{13}^{-01}\right), \\ &hE_{33}^{10} = A_1\bar{\varsigma}_1\left(E_{13}^{+00} - E_{13}^{-00}\right), \quad hE_{33}^{01} = A_2\bar{\varsigma}_2\left(E_{23}^{+00} - E_{23}^{-00}\right). \end{aligned} \tag{18}$$

Eq. (18) imply that only seven aforementioned higher approximation modes are independent of 11 higher approximation modes of strains.

The governing equations for the element e are obtained by applying the Hu–Washizu variational principle. Using Eqs. (14)–(18), and eliminating the strain and stress resultant parameters on the element level, one can obtain

$$\mathbf{KU} = \mathbf{R},$$

where $\mathbf{K}$ is the elemental stiffness matrix, $\mathbf{R}$ is the load vector, $\mathbf{U}$ is the vector of the six displacement components at nodal points of the element.

It should be noted that the formulation of the stiffness matrix $\mathbf{K}$ requires only direct substitutions; no inversion is needed if the element is rectangular. The matrix is symmetric and positive definite, and has six, and only six, zero eigenvalues as required for satisfaction of the general rigid body motion representation. Furthermore, the element matrix can be evaluated by using the full exact integration if geometrical parameters are constant inside the element, and the element does not contain any spurious zero energy modes, and, finally, the element passes the patch test [17] which requires accommodation of the homogeneous states of strains.

6. Numerical tests

Four tests were employed to assess the effectiveness of this element. They are a thin rectangular plate test, a pinched cylindrical shell test, an isotropic open cylindrical shell roof test, and a multilayered composite open cylindrical shell test.

6.1. Thin plate test

This classical elastic problem has been widely used by many investigators (see, for example [3,16]) as a benchmark test for the bending plate element behaviour. The geometrical and mechanical properties and the used meshes of a rigidly clamped rectangular plate subjected to uniform (UL) and concentrated (CL) loads are shown in Fig. 4. Due to symmetry only one quadrant is discretized. Figs. 5 and 6 present the dependence of the central transverse displacement $v_3^M(0,0)$ normalized with respect to the Kirchhoff plate solution $v_3^K(0,0)$ [30] on the number of elements N_e. The curves marked by T1 and U1 have been obtained by Hughes and Tezduyar [16], where T1 denotes the assumed strain plate element that possesses a correct rank while U1 denotes the traditional plate element based on the uniform reduced integration that possesses four spurious zero energy modes. The results marked by ∘ have been calculated on the basis of our approach. It can be seen that all elements perform well.

6.2. Pinch test

The pinched cylinder (see Fig. 7) has been extensively treated for the numerical testing of new finite-element models. The radial deflection $w_{\max}$ at the load P is given in Fig. 8. The curves marked by ∘

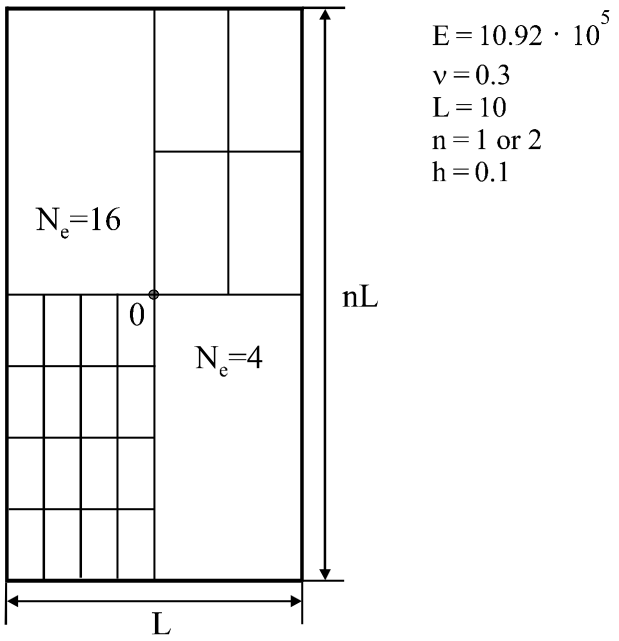

Fig. 4. Thin clamped rectangular plate.

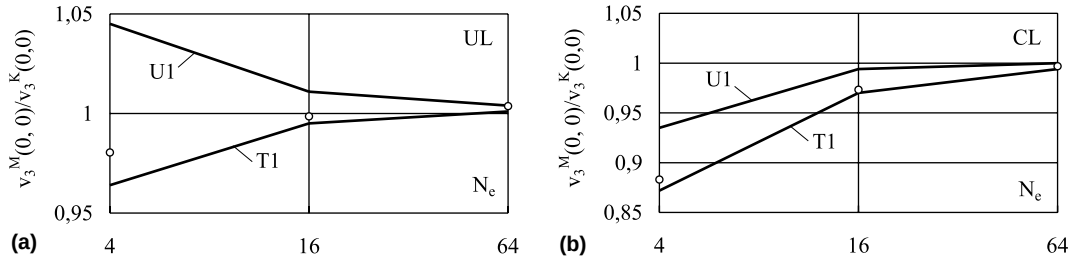

Fig. 5. Clamped square ($n = 1$) plate: (a) uniform load and (b) concentrated load. Comparison with T1 and U1 Mindlin plate elements [16].

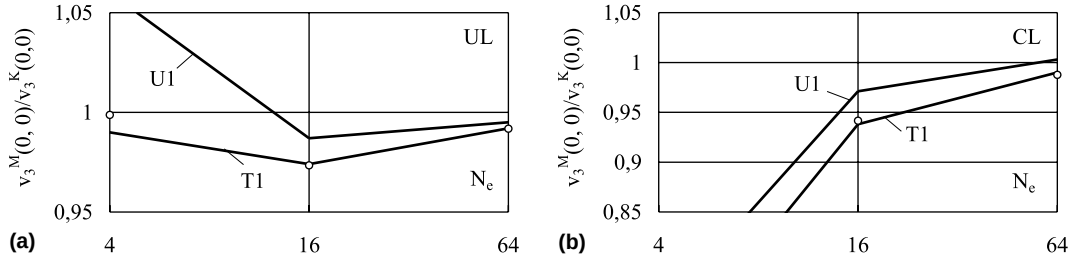

Fig. 6. Clamped rectangular ($n = 2$) plate: (a) uniform load and (b) concentrated load. Comparison with T1 and U1 Mindlin plate elements [16].

display the results obtained by using the above element taking into account the transverse shear strains only, i.e., $v_3^- = v_3^+ = v_3$. Additionally, in Fig. 8(a) the solutions, based on the traditional cubic Lagrange element (see curves marked by ♢) and the cubic Lagrange element [13] which has been augmented in

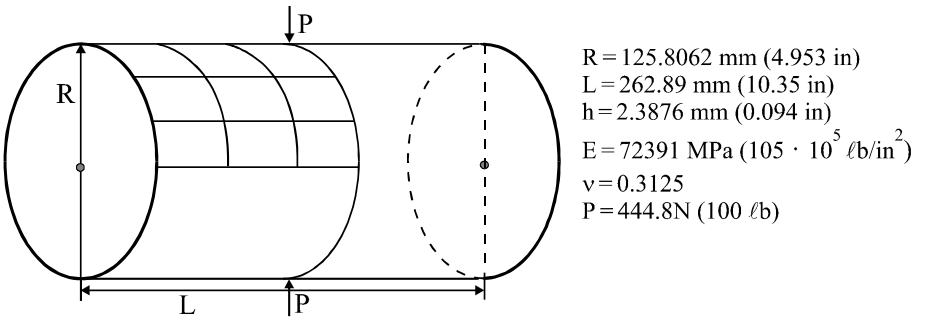

Fig. 7. Pinch test: Cylindrical shell under radial forces with free edges.

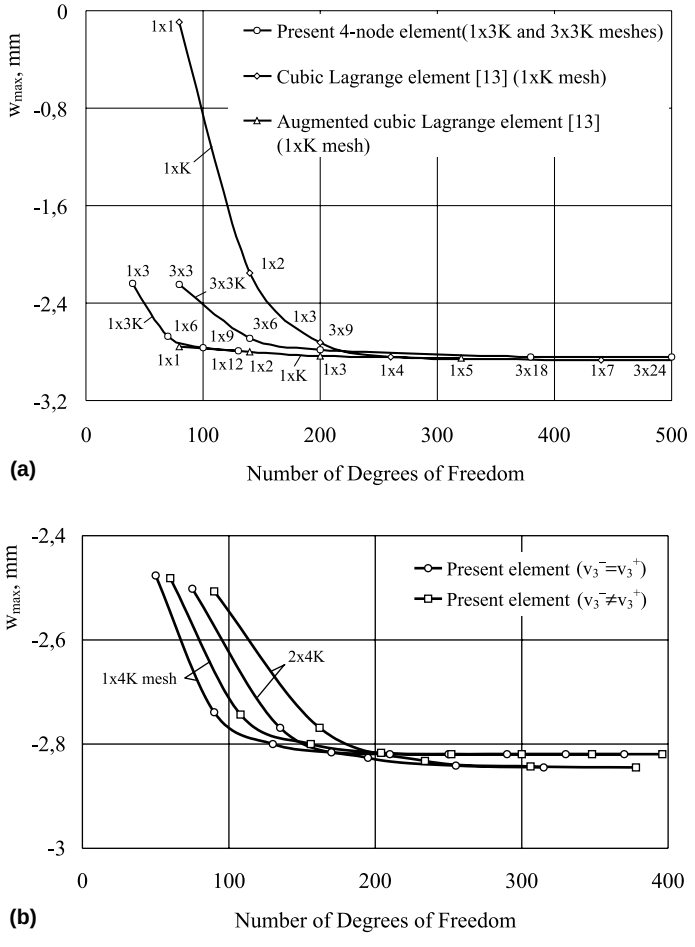

Fig. 8. Pinch test: Radial deflection under load: (a) comparison with traditional cubic Lagrange TMT shell element solutions and (b) comparison of both present finite-element solutions.

the manner of [9] to provide the correct rigid body motions (see curves marked by △), are presented. Both Lagrange elements are based on the classical TMT shell theory. Note that the augmented Lagrange element solution converges to a value of $w_{\max} = -2.830$ mm [13] as do the present 4-node element and the cubic Lagrange element. However, our simple and efficient element solution converges more rapidly, since the cubic Lagrange element possesses only two zero eigenvalues. At the same time

its augmented formulation has the six zero eigenvalues as required for satisfaction of the general rigid body motion requirements. Fig. 8(b) displays the results obtained by using both present finite-element solutions, where curves marked by □ show a solution with account of the transverse normal effect, i.e., $v_3^- \neq v_3^+$.

6.3. Roof test

Consider an open cylindrical shell segment (see Fig. 9) subjected to the gravitational self-weight loading and supported at its curved edges by rigid diaphragms while the straight edges are free. This problem has been also used frequently for numerical testing of finite-element approximations. Fig. 10 shows the distribution of the axial displacement at the diaphragm (around the curve AD) and the vertical displacement at the middle span (around the curve BC) while Fig. 11 displays the distribution of the moment resultants $M_{\alpha\alpha} = h(H_{\alpha\alpha}^+ - H_{\alpha\alpha}^-)/2$ at the middle span. The solid curves show the results obtained by using the exact solution [28] as reported in works [1,32]. The results marked by Δ, ◇ and ○ have been computed on the basis of the developed 4-node element taking into account the transverse shear strains only ($v_3^- = v_3^+ = v_3$). Note that results for the 8×12 mesh (see Fig. 10) are better to those given in above works for the 4×6 mesh of fully integrated parabolic serendipity elements. As can be seen in Fig. 11, the moment resultant M_{11} is calculated with an excellent exactitude for both meshes. While the results obtained for the moment resultant M_{22} are less satisfactory. This phenomenon is explained by using the constant approximation over the

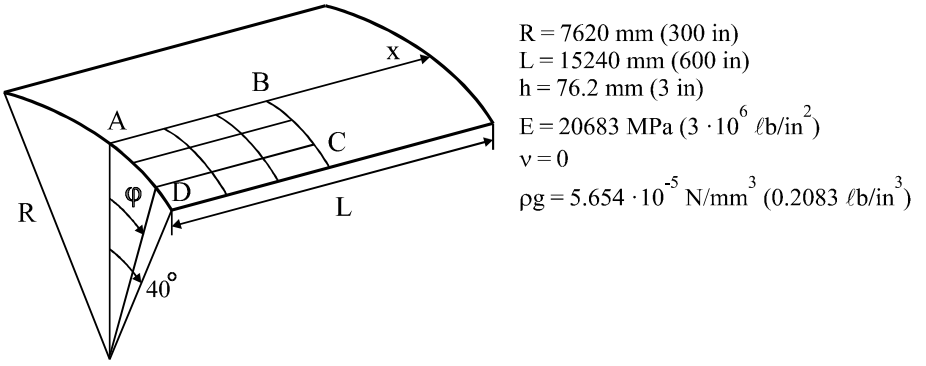

Fig. 9. Roof test: Open cylindrical shell under self-weight loading.

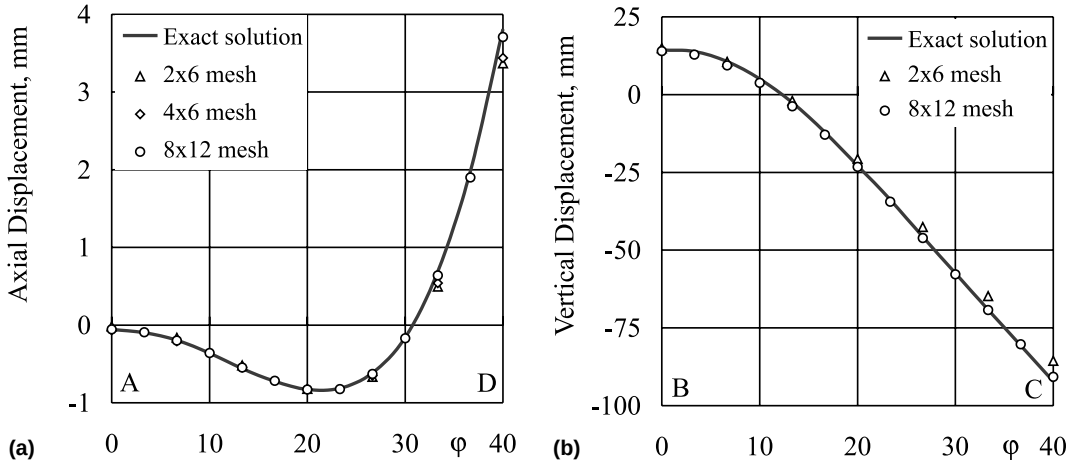

Fig. 10. Roof test: Displacements at: (a) diaphragm and (b) middle span.

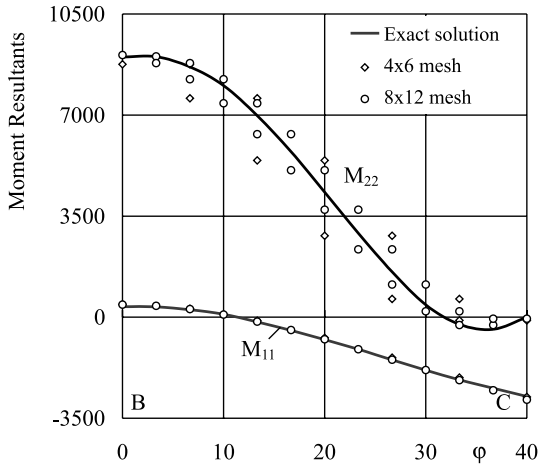

Fig. 11. Roof test: Moment resultants at middle span.

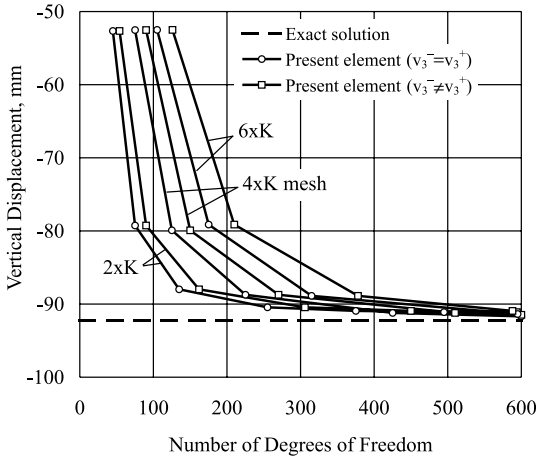

Fig. 12. Roof test: Vertical displacement at point C: comparison of both present finite-element solutions.

element for the generalized stress resultants $H_{22}^{\pm}$ in the φ direction in accordance with Eq. (17). In addition, Fig. 12 presents the dependence of the vertical displacement at the point C of a middle span on the number of degrees of freedom. The curves marked by ○ and □ show the results based on both developed elements allowing for the transverse shear strains and transverse normal strains. One can see that our simple 4-node elements give good results.

6.4. Composite shell test

It is apparent that using the simplified strain–displacement Eq. (4) may lead to incorrect results for the composite shells. To assess this statement, we consider an open cylindrical two-layered anisotropic shell rigidly clamped at its curved edges and supported at straight edges by rigid diaphragms. The shell is subjected to the uniform stretching v_0 as shown in Fig. 13. The material characteristics of each layer were taken to be those typical of a high modulus composite [12,21] and are given in Fig. 13, where the subscripts L, T and Z refer to the longitudinal, transverse and thickness directions of the individual ply. Let the ply thicknesses and ply orientations be $[h/2, h/2]$ and $[-\gamma, +\gamma]$, where γ is measured in the clockwise direction

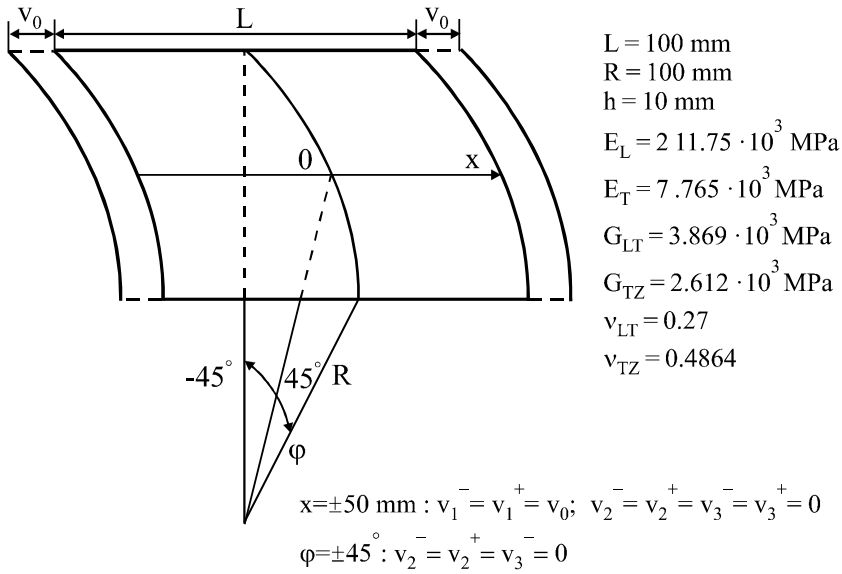

Fig. 13. Composite shell test.

Table 1
Transverse displacement of the middle surface $-(v_3^- + v_3^+)/2v_0$ in a centre of the shell segment

Variant	Strain–displacement equation (3)				Strain–displacement equation (4)			
	Ply orientations				Ply orientations			
	[0°, 90°]	[− 15°, 15°]	[−30°, 30°]	[−60°, 60°]	[0°, 90°]	[−15°, 15°]	[−30°, 30°]	[−60°, 60°]
4 × 4 mesh	0.071	1.585	4.062	1.390	0.072	1.584	4.058	1.391
4 × 8 mesh	0.056	1.269	3.366	1.198	0.057	1.268	3.362	1.198
4 × 12 mesh	0.053	1.255	3.309	1.158	0.054	1.254	3.306	1.158
8 × 8 mesh	0.049	1.367	3.526	1.125	0.050	1.365	3.519	1.124
8 × 16 mesh	0.045	1.343	3.444	1.068	0.046	1.342	3.438	1.067
8 × 24 mesh	0.044	1.339	3.430	1.055	0.045	1.337	3.424	1.054
12 × 12 mesh	0.048	1.365	3.486	1.074	0.046	1.363	3.480	1.073
12 × 24 mesh	0.043	1.354	3.451	1.045	0.044	1.353	3.445	1.043

from x to the fiber direction. In Table 1 the values of the dimensionless transverse displacement of the middle surface in a centre of the shell segment for both strain–displacement equations (3) and (4), and for various ply orientations and meshes are presented. It can be seen that using the strain–displacement equation (3) only insignificantly updates the results in a comparison with less general strain–displacement equation (4). Thus, the geometrically linear theory of shells on the basis of strain–displacement equation (4), it is possible to recommend for using in engineering calculations. At the same time applying the strain–displacement relationships, that are not completely free for rigid body motions, for solving the composite shells undergoing the large deformations can lead to significant errors. Such a problem is currently under development.

Finally, Fig. 14 shows the distribution of the thickness variation $\Delta h = v_3^+ - v_3^-$ at $x = 0$ and ± 25 mm in φ direction. As can be seen, a response of the shell is very unusual to $x = 0$ and ply orientation $[-30°, 30°]$. In this case the thickness variation Δh is positive and has a maximum value at $\varphi = 0$. Note that a similar result for the axisymmetric cylindrical two-layered anisotropic shell has been recently reported in [20].

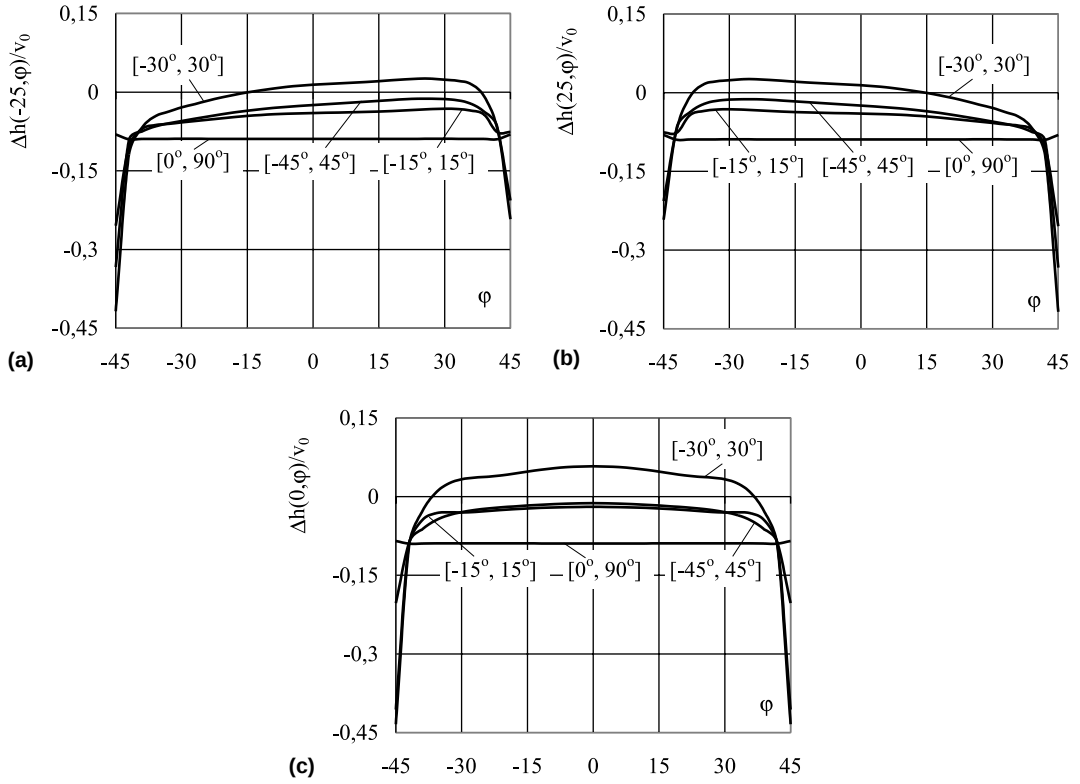

Fig. 14. Distribution of thickness variation $\Delta h = v_3^+ - v_3^-$ at (a) $x = -25$ mm, (b) $x = 25$ mm and (c) $x = 0$ in φ direction.

7. Conclusions

The simple and efficient mixed models have been developed for the analysis of multilayered anisotropic TMT shells. The first finite-element formulation is based on the strain–displacement equations of the *moderately thick* shell, which are completely free for rigid body motions. The second finite-element formulation is based on the strain–displacement equations of the *thin* shell, which cannot be completely free for rigid body motions in the case of anisotropic shells of arbitrary geometry. As fundamental unknowns six displacements and eleven strains of the face surfaces of the shell, and 11 stress resultants have been chosen.

The elemental stiffness matrices of our formulation are symmetric and positive definite, and have six zero eigenvalues as required for satisfaction of the general rigid body motion representation. Besides, the elemental matrices require only direct substitutions (no inversion is needed) if elements are rectangular, and they can be evaluated using the full exact integration. The elements do not contain any spurious zero energy modes and they pass the patch test which requires accommodation of the homogeneous states of strains.

To demonstrate the high accuracy and effectiveness of the developed finite-element models, four tests were employed. They were a thin rectangular plate test, a pinch test, an open cylindrical shell segment roof test and an open cylindrical composite shell segment test.

The extension to finite deflections poses no additional difficulties but requires algebra and computation efforts. For this purpose the Hu–Washizu mixed functional for an analysis of geometrically non-linear multilayered anisotropic shells [18,21] can be used. The extension to initially stressed multilayered shells can be also done [19].

Acknowledgements

The present research was supported by Deutsche Forschungsgemeinschaft and Russian Fund of Basic Research (Grant No. 98-01-04076) and by Research Programme of Tambov State Technical University (Grants No. 5Г-99 and 1Г/00-10).

References

[1] S. Ahmad, B.M. Irons, O.C. Zienkiewicz, Analysis of thick and thin shell structures by curved finite elements, Int. J. Numer. Meth. Eng. 2 (3) (1970) 419–451.
[2] K.J. Bathe, Finite Element Procedures, Prentice-Hall, Englewood Cliffs, NJ, 1996.
[3] K.J. Bathe, E.N. Dvorkin, A 4-node plate bending element based on Mindlin/Reissner plate theory and a mixed interpolation, Int. J. Numer. Meth. Eng. 21 (2) (1985) 367–383.
[4] T. Belytschko, W.K. Liu, J.S.J. Oug, D. Lam, Implementation and application of a 9-node Lagrange shell element with spurious mode control, Comput. Struct. 20 (1–3) (1985) 121–128.
[5] T. Belytschko, H. Stolarski, W.K. Liu, N. Carpenter, J.S.J. Oug, Stress projection for membrane and shear locking in shell finite elements, Comput. Methods Appl. Mech. Engrg. 51 (1-3) (1985) 221–258.
[6] P. Betsch, E. Stein, An assumed strain approach avoiding artificial thickness straining for a nonlinear 4-node shell element, Commun. Numer. Meth. Eng. 11 (1995) 899–909.
[7] M. Bischoff, E. Ramm, Shear deformable shell elements for large strains and rotations, Int. J. Numer. Meth. Eng. 40 (23) (1997) 4427–4449.
[8] G. Cantin, Strain displacement relationships for cylindrical shells, AIAA J. 6 (9) (1968) 1787–1788.
[9] G. Cantin, Rigid body motions in curved finite elements, AIAA J. 8 (7) (1970) 1252–1255.
[10] D.J. Dawe, Rigid-body motions and strain–displacement equations of curved shell finite elements, Int. J. Mech. Sci. 14 (9) (1972) 569–578.
[11] A.L. Gol'denveiser, Theory of Elastic Thin Shell, Pergamon Press, Oxford, 1961.
[12] E.I. Grigolyuk, G.M. Kulikov, Multilayered Reinforced Shells: Analysis of Pneumatic Tires, Mashinostroyenie, Moscow, 1988 (in Russian).
[13] J.S. Hansen, G.R. Heppler, A Mindlin shell element that satisfies rigid-body requirements, AIAA J. 23 (2) (1985) 288–295.
[14] T.J.R. Hughes, The Finite Element Method: Linear Static and Dynamic Finite Element Analysis, Prentice-Hall, Englewood Cliffs, NJ, 1987.
[15] T.J.R. Hughes, R.L. Taylor, W. Kanok-Nukulchai, A simple and efficient finite element for plate bending, Int. J. Numer. Meth. Eng. 11 (10) (1977) 1529–1543.
[16] T.J.R. Hughes, T.E. Tezduyar, Finite elements based upon Mindlin plate theory with particular reference to the 4-node bilinear isoparametric element, J. Appl. Mech. 48 (3) (1981) 587–596.
[17] B.M. Irons, A. Razzaque, Experience with the patch test for convergence of finite elements, in: A.K. Aziz (Ed.), The Mathematical Foundations of the Finite Element Method with Applications to Partial Differential Equations, Academic Press, New York, 1972, pp. 557–587.
[18] G.M. Kulikov, Variational equation for the non-linear multilayered anisotropic shell of variable stiffness, Trans. Tambov State Technical University 3 (1–2) (1997) 119–125.
[19] G.M. Kulikov, Analysis of initially stressed multilayered shells, Int. J. Solids Struct. 38 (26–27) (2001) 4535–4555.
[20] G.M. Kulikov, Refined global approximation theory of multilayered plates and shells, J. Eng. Mech. 127 (2) (2001) 119–125.
[21] G.M. Kulikov, S.V. Plotnikova, Comparative analysis of two algorithms for numerical solution of non-linear static problems for multilayered anisotropic shells of revolution, 1. Account of transverse shear, Mech. Compos. Mater. 35 (3) (1999) 241–248.
[22] G.M. Kulikov, S.V. Plotnikova, Comparative analysis of two algorithms for numerical solution of non-linear static problems for multilayered anisotropic shells of revolution 2. Account of transverse compression, Mech. Compos. Mater. 35 (4) (1999) 293–300.
[23] L. Librescu, Elastostatics and Kinetics of Anisotropic and Heterogeneous Shell-Type Structures, Noordhoff, Leyden, 1975.
[24] D.S. Malkus, T.J.R. Hughes, Mixed finite element methods-reduced and selective integration techniques: a unification of concepts, Comput. Methods Appl. Mech. Engrg. 15 (1) (1978) 63–81.
[25] R.D. Mindlin, Influence of rotatory inertia and shear on flexural motions of isotropic elastic plates, Trans. ASME J. Appl. Mech. 18 (1) (1951) 31–38.
[26] T.H.H. Pian, P. Tong, Basis of finite element methods for solid continua, Int. J. Numer. Meth. Eng. 1 (1) (1969) 3–28.
[27] J.N. Reddy, Mechanics of Laminated Composite Plates: Theory and Analysis, CRC Press, Boca Raton, FL, 1997.
[28] A.C. Scordelis, K.S. Lo, Computer analysis of cylindrical shells, Am. Conc. Inst. J. 61 (5) (1964) 539–560.
[29] S.P. Timoshenko, On the correction for shear of the differential equation for transverse vibrations of prismatic bars, Philos. Mag. J. Sci. Ser. 6 41 (245) (1921) 744–746.
[30] S.P. Timoshenko, S. Woinowsky-Krieger, Theory of Plates and Shells, McGraw-Hill, New York, 1959.
[31] G. Wempner, D. Talaslidis, C.M. Hwang, A simple and efficient approximation of shells via finite quadrilateral elements, Trans. ASME J. Appl. Mech. 49 (1) (1982) 115–120.
[32] O.C. Zienkiewicz, R.L. Taylor, J.M. Too, Reduced integration technique in general analysis of plates and shells, Int. J. Numer. Meth. Eng. 3 (2) (1971) 275–290.